Direct measurements of conductivity and mobility in millimeter-sized single-crystalline graphene via van der Pauw geometry*

Rui-Song Ma(马瑞松)[1,2,3], Qing Huan(郇庆)[1,2,3], Liang-Mei Wu(吴良妹)[1,2,3], Jia-Hao Yan(严佳浩)[1,2,3], Yu-Yang Zhang(张余洋)[2], Li-Hong Bao(鲍丽宏)[1,2,3,†], Yun-Qi Liu(刘云圻)[4], Shi-Xuan Du(杜世萱)[1,2,3], and Hong-Jun Gao(高鸿钧)[1,2,3,‡]

[1] *Institute of Physics & School of Physical Sciences, University of Chinese Academy of Sciences (CAS), Beijing* 100190, *China*
[2] *CAS Key Laboratory of Vacuum Physics, University of Chinese Academy of Sciences, Beijing* 100049, *China*
[3] *Beijing Key Laboratory for Nanomaterials and Nanodevices, Beijing* 100190, *China*
[4] *Institute of Chemistry, Chinese Academy of Sciences, Beijing* 100190, *China*

(Received 14 March 2017; revised manuscript received 10 April 2017; published online 10 May 2017)

We report the direct measurements of conductivity and mobility in millimeter-sized single-crystalline graphene on SiO_2/Si via van der Pauw geometry by using a home-designed four-probe scanning tunneling microscope (4P-STM). The gate-tunable conductivity and mobility are extracted from standard van der Pauw resistance measurements where the four STM probes contact the four peripheries of hexagonal graphene flakes, respectively. The high homogeneity of transport properties of the single-crystalline graphene flake is confirmed by comparing the extracted conductivities and mobilities from three setups with different geometry factors. Our studies provide a reliable solution for directly evaluating the entire electrical properties of graphene in a non-invasive way and could be extended to characterizing other two-dimensional materials.

Keywords: graphene conductivity, mobility, four-probe measurement, van der Pauw method

PACS: 68.37.Ef, 81.15.Gh, 72.80.Vp **DOI:** 10.1088/1674-1056/26/6/066801

1. Introduction

Graphene, a two-dimensional (2D) semimetal with honeycomb structure,[1] has attracted considerable attention in science and engineering community because of its excellent mechanical,[2] electrical,[3] and optical[4] properties, and potential applications such as field-effect transistors (FETs),[3,5] solar cells,[6] and flexible and transparent electrodes.[7] The typical growth method of large-scale and high-quality graphene is the chemical vapor deposition (CVD) by using a transition metal as substrates, such as Ni[7] and Cu[8] foils. After transferring to a dielectric substrate, such as SiO_2/Si wafer, traditional two-terminal[5,9] or four-terminal[10,11] methods are adopted to measure the electrical transport properties. Among the four-terminal methods, which could eliminate the contact and electrode resistance,[12] van der Pauw geometry is commonly used to extract the resistivity and Hall coefficient of a 2D sample with arbitrary shape.[13,14] In the van der Pauw method, four electrodes are located on the sample periphery, and the resistivity or conductivity of the arbitrary-shaped 2D sample can be determined just from two simple resistance measurements.[13,14]

However, in traditional "off-line" measurements, including two- and four-terminal methods, lithographically defined electrodes are needed,[9–11,15] which could contaminate the samples. In contrast, the four-probe measurement performed by the four-probe scanning tunneling microscope (4P-STM) system in ultra-high vacuum (UHV),[16,17] can avoid contamination and preserve the original shapes and properties of the samples after being characterized. Moreover, the 4P-STM system can realize the combination of high-resolution positioning[18] and transport measurement simultaneously.[16,19] With the extremely sharp STM probes as electrodes, the measurements will do the least damage to the sample. Nevertheless, measurements of graphene conductivity and mobility by direct four-probe method have been rarely reported.[20,21]

In this work, we investigate the direct measurement of transport properties of CVD-grown millimeter-sized single-crystalline graphene by a home-designed 4P-STM via van der Pauw geometry. We find that the conductivities of graphene, measured from three setups, show high homogeneity despite the geometry difference in probe positions. The extracted mobilities from the gate tunable conductivity show relatively high

*Project supported by the Science Fund from the Ministry of Science and Technology of China (Grant No. 2013CBA01600), the National Key Research & Development Project of China (Grant No. 2016YFA0202300), the National Natural Science Foundation of China (Grant Nos. 61474141, 61674170, 61335006, 61390501, 51325204, and 51210003), the Chinese Academy of Sciences (CAS), and Youth Innovation Promotion Association of CAS (Grant No. 20150005).

†Corresponding author. E-mail: lhbao@iphy.ac.cn
‡Corresponding author. E-mail: hjgao@iphy.ac.cn

© 2017 Chinese Physical Society and IOP Publishing Ltd

values, which are in a range of about 4000 $cm^{-2}\cdot V^{-1}\cdot s^{-1}$ ~ 5000 $cm^{-2}\cdot V^{-1}\cdot s^{-1}$. Despite the graphene wrinkles and multilayered flakes that are distributed randomly on the single-crystalline monolayer graphene, both the conductivity and mobility show almost the same values from the three different setups. This verifies the robustness of our measurement method. Our measurements demonstrate a reliable way to obtain graphene conductivity and mobility, and may be extended to evaluating the electrical properties of other 2D materials.

2. Methods

The graphene samples were grown on Cu foil by the CVD method.[8] The STM characterization and atomic force microscopy (AFM) characterization are carried out in air at ambient temperature by the Nanoscope IIIa SPM (Digital Instruments). The STM images were acquired in constant current mode and AFM images were obtained in the tapping mode. The millimeter-sized single-crystalline graphene flakes were then transferred onto SiO_2/Si wafer by the poly (methyl, methacrylate)-assisted method.[8] Raman spectra were measured by using a Horiba Jobin Yvon LabRAM HR-800 Raman microscope at ambient temperature and pressure (laser wavelength = 532 nm, power = 1 mW, beam spot = 1 μm). The electrical transport measurements were carried out by a home-designed UHV four-probe STM system. Before transport characterization, the samples of graphene on SiO_2/Si were annealed at 500 K for 24 hours at a pressure of $\sim 1\times10^{-7}$ Pa in the STM chamber. The capacitance between the probes and the gate electrode, rather than tunneling current, are monitored as real-time feedback signals for the probes to approach to the sample automatically. All four-probe characterizations were performed at room temperature in the UHV chamber with a base pressure of about 5×10^{-8} Pa, and the electrical properties were measured by a Keithley 4200-SCS system.

3. Results and discussion

Single-crystalline graphene flakes with hexagonal shape can be easily found and the grain size can be as large as several millimeters as shown in Fig. 1(a). STM characterization has been carried out to verify the continuity and quality of graphene grown on Cu foil. Large-area scans of graphene-covered Cu foil substrates collected at different positions show varied surface topography features. Figure 1(b) shows the typical morphology of graphene on Cu foil, which reveals the highly-corrugated substrate that is full of irregular steps, small islands and pits. Two atomically-resolved STM images are shown in Figs. 1(c) and 1(d), respectively. The continuous triangular lattices maintain the same orientation across highly-corrugated features of the Cu surface underneath. The occurrence of triangular lattices rather than honeycomb structures in the STM images could be attributed to the highly-corrugated substrate surface, which leads to uneven strain effects and the breaking of the six-fold symmetry of the graphene carbon lattice.[22] Another large-area STM image in Fig. S1(a) in the supporting information (see Appendix A) shows a topography with triangular and parallelogram features. The graphene also maintains a continuous pristine atomic structure over steps, edges, vertices and flat plane of the copper surface (as shown in Figs. S1(c)–S1(f) in Appendix A). Other irregular morphologies together with their high-resolution STM images are shown in Fig. S2 (see Appendix A). All the STM characterizations verify the continuity and high quality of the graphene over these different copper surface structures.

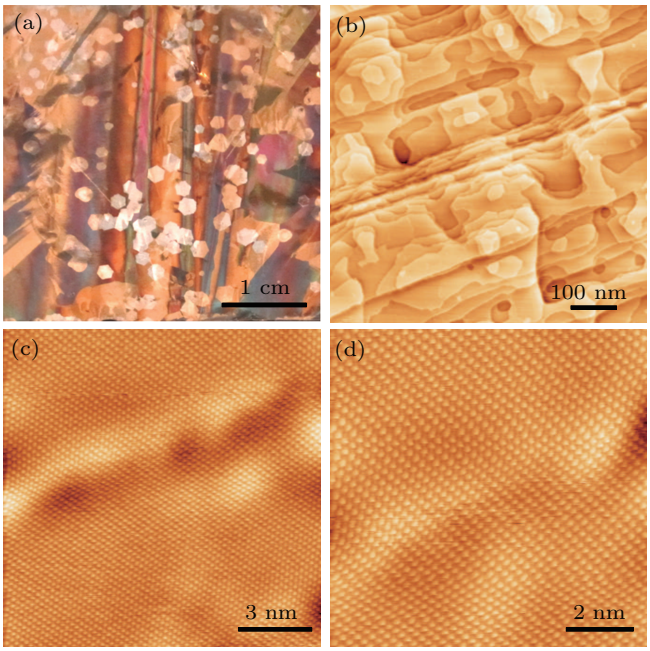


Fig. 1. (color online) Optical and STM characterization of graphene grown on Cu foil. (a): Optical photograph of graphene grown on Cu foil by CVD method. The scale bar is 1 cm and the grain size of the graphene grain is in the range of millimeter. (b): STM image showing one of the graphene-covered Cu foil. (c)–(d): Atomically-resolved STM images on the morphology in panel (b). Scanning conditions, (b)–(d): I_t = 367.3 pA and V_{sample} = 82.02 mV.

An optical micrograph of a transferred monolayer graphene flake onto SiO_2/Si substrate is shown in Fig. 2(a), wherein the optical contrast verifies its monolayer nature.[3,23] Raman spectra of this hexagonal graphene are collected at four different positions (numbered by 1–4 in Fig. 2(a)) with an excitation wavelength of 532 nm of the laser as shown in Fig. 2(b). The relative intensity ratio of 2D and G peaks (> 2 : 1) confirms the monolayer nature of this single-crystalline graphene flake.[24] Furthermore, the absence of the D peak reveals that the transferred graphene sample on the SiO_2/Si substrate has no detectable defects.

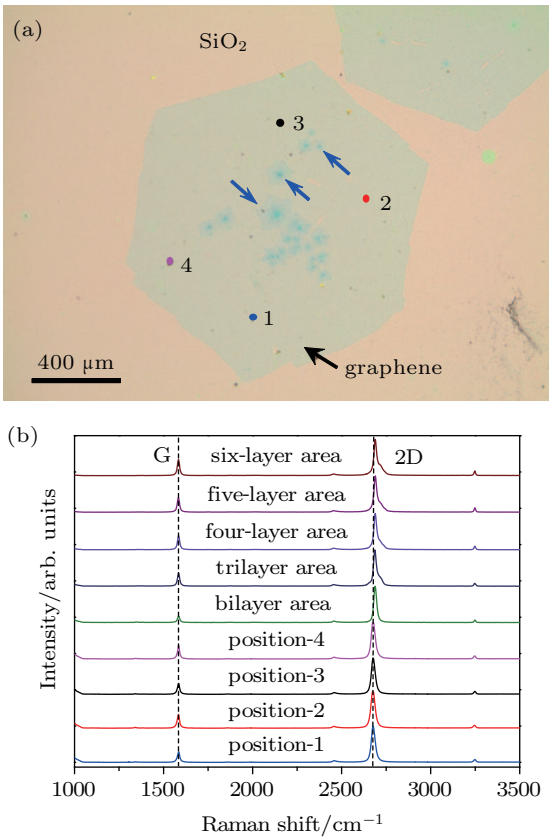


Fig. 2. (color online) Optical and Raman characterization of monolayer graphene transferred onto SiO_2/Si substrate. (a): Optical micrograph of a monolayer graphene flake on SiO_2/Si. Small multilayer flakes indicated by blue arrows are distributed randomly on this millimeter-sized graphene flake. (b): Raman spectra collected on four monolayer positions and multilayers of this graphene flake. The four monolayer positions are indicated by four numbered circles in panel (a) and the positions collected on multilayers are shown in Fig. S5(a) in Appendix A. The excitation wavelength of the laser is 532 nm. The spectra are offset vertically for clarity.

In traditional van der Pauw measurements, four electrodes are fabricated to contact the edge of the original material flake[25] or the etched sample.[10,11] To preserve the original shapes and properties of the samples, the four probes of the 4P-STM directly contact with the four peripheries of hexagonal graphene flake. There are three different measurement setups as shown in Fig. 3. The four chemically-etched gold probes are denoted as probes 1–4 and form a rectangle indicated by white dash lines. Optical micrographs of the probes and sample in the three setups during measurements are shown in Fig. S3 in Appendix A. In each setup, two testing configurations $I1_V23$ and $I2_V34$ are used during measurements. The configuration $I1_V23$ is defined as follows: Probe 1 (current probe) injects the current ($I1$), probe 4 (current probe) is grounded, while probes 2 and 3 (voltage probes) measure the potential difference between them ($V23 = V2 - V3$). The configuration $I2_V34$ can be understood in the same way as $I1_V23$. The measured resistance is defined by $V23/I1$ (R_{I1_V23}) and $V34/I2$ (R_{I2_V34}) for $I1_V23$ and $I2_V34$, respectively.

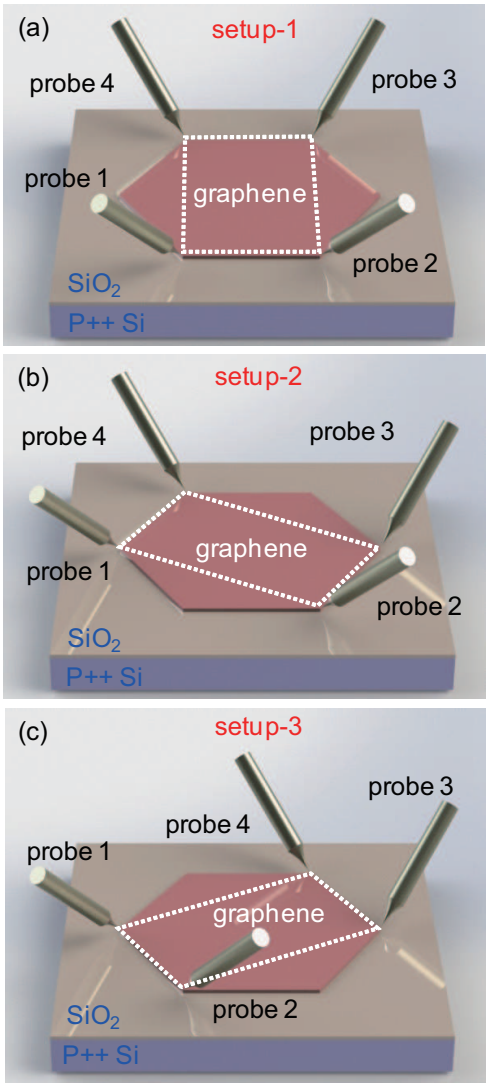


Fig. 3. (color online) Schematic diagrams of direct four-probe measurements on graphene via van der Pauw geometry. (a): Schematic diagram of four-probe measurement by setup-1. Probe 1 and 2 contact two nearest corners while probe 3 and 4 contact the corners on the opposite side. (b)–(c): Schematic diagrams of setup-2 and setup-3, respectively. The rectangles formed by the probes in these two setups are rotated relative to that in setup-1 with $-2\pi/3$ and $2\pi/3$, respectively.

The measured resistances as a function of gate voltage for the three setups are presented in Figs. 4(a)–4(c). In all the setups, two configurations ($I1_V24$ and $I2_V34$) give different measured resistances which result from the geometry inhomogeneity, i.e., the spacings between the current probes and voltage probes are different. The Dirac points are all located at ~ -6 V, which indicates an n-doped nature of the graphene flake. The n-doped feature originates from two aspects. First, the vacuum annealing process leads to the desorption of PMMA residue from the surface and the potentially trapped molecules, such as H_2O and O_2, at the graphene/SiO_2 interface, i.e., the source of p-type doping is removed.[26] Second, the n-doping effect on graphene is due to the low work function of the substrate as well as the chemicals generated by the vacuum ion gauge.[27]

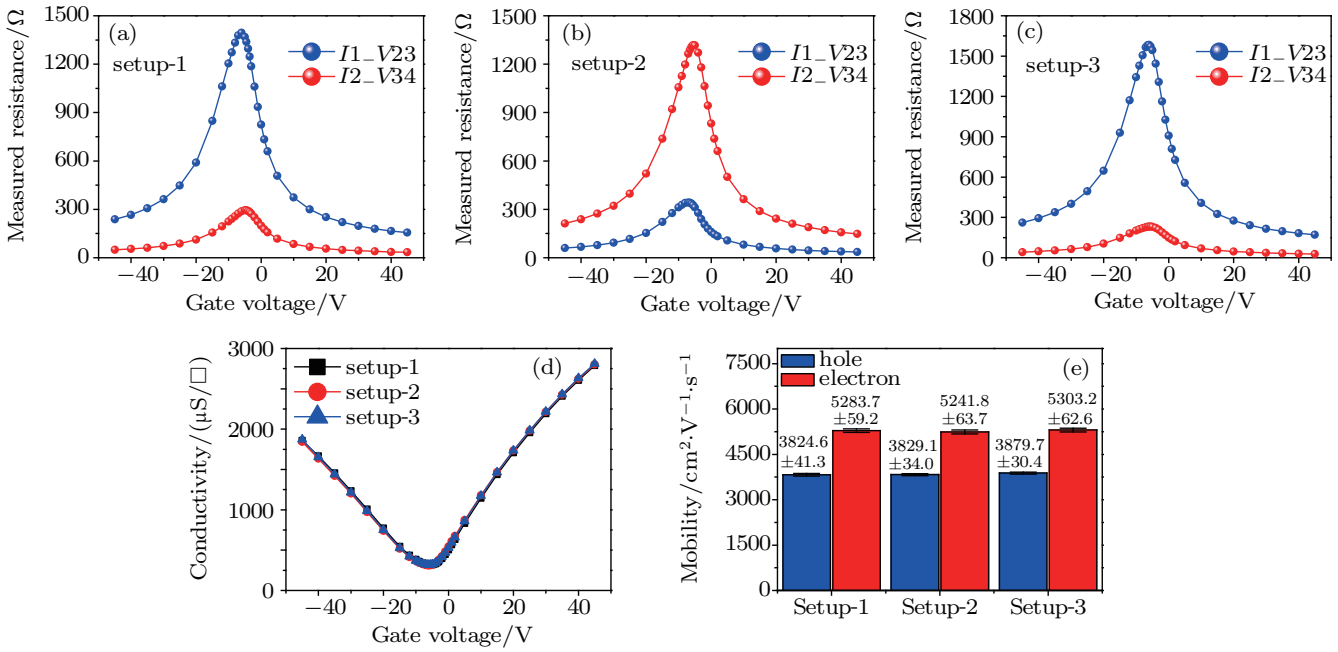


Fig. 4. (color online) Conductivity and mobility of graphene by direct four-probe measurements via van der Pauw geometry. (a)–(c): Measured resistance by setup-1, setup-2, and setup-3, respectively. Curves from configurations *I*1_*V*23 and *I*2_*V*34 are indicated by blue and red colors, respectively. (d): Conductivity of the graphene flake in Fig. 2 calculated from the three setups. The fact that the three curves nearly coincide with each other demonstrates the homogeneity of transport properties of this graphene flake. (e): Extracted hole and electron mobility for the three setups.

According to van der Pauw theory,[13,14] the conductivity $\sigma_{\square}$ of the graphene flake can be calculated from the two configurations by the equation

$$1/\sigma_{\square} = \frac{\pi}{\ln 2}\frac{R_{I1_V23}+R_{I2_V34}}{2}f, \tag{1}$$

where the factor f is a function of ratio R_{I1_V23}/R_{I2_V34}. As shown in Fig. 4(d), the curves of conductivity versus gate voltage for the three setups almost coincide with each other, which indicates the homogenous transport properties of the single-crystalline graphene flake. The mobility μ can be derived according to the equation[9,28]

$$\mu = \frac{1}{C_{\rm OX}}\frac{{\rm d}\sigma_{\square}}{{\rm d}V_{\rm g}}, \tag{2}$$

where $V_{\rm g}$ is the gate voltage and $C_{\rm OX}$ is the capacitance per unit area of the dielectric layer of the wafer. In our case, the thickness of the SiO_2 layer is 300 nm and thus the $C_{\rm OX}$ is 1.15×10^{-8} F·cm^{-2}.[28] The hole and electron mobility can be extracted by linearly fitting the conductivity curves on left and right part in Fig. 4(d), respectively.[5,15] The calculated hole and electron mobility values from the three setups are summarized in Fig. 4(e). The hole mobility values in units cm^{-2}·V^{-1}·s^{-1}are 3824.6±41.3, 3829.1±34.0, and 3879.7±30.4, while those for the electron are 5283.7±59.2, 5241.8±63.7, and 5303.2±62.6 for setup-1, setup-2, and setup-3, respectively. These values are consistent with previous results from graphene FET devices.[8] Furthermore, these mobilities extracted from the three different setups show nearly no difference within measurement error. Due to its honeycomb structure, pristine graphene is expected to show isotropic transport properties in plane,[29] which is consistent with our results.

Finally, it should be mentioned that although there are graphene wrinkles and multilayers distributed randomly on the monolayer graphene, their presence does not destroy the homogeneity of transport properties nor introduce obvious anisotropy in the measurements. AFM characterizations of both edges and central regions of graphene flake confirm that the graphene wrinkles are randomly distributed (as shown in Fig. S4 in Appendix A). According to previous studies, the graphene wrinkles would either impede the charge transport and thus bring additional resistance,[30] or even enhance the conductivity compared with pristine graphene.[31] In addition, there are several small multi-layer graphene flakes distributed on the large monolayer graphene as shown in Fig. 2(a). The layer number can be as large as six as revealed by the zoom-in optical micrographs (as shown in Fig. S5 in Appendix A). According to previous studies,[32] these small graphene multilayers are positioned beneath the topmost graphene layer. The Raman spectra collected on one typical multi-layer graphene flake (see Fig. S5(a) in Appendix A) are shown in Fig. 2(b). Comparing with monolayer area, the 2D peak collected on the bilayer graphene area still shows symmetrical one-peak feature, but a blue shift about 10 cm^{-1} and a substantial increase

in the I_{2D}/I_G ratio (~ 5.6) are observed. This can be attributed to the twisting between graphene layers, which could lead to the decoupling of the electronic structure.[33] We also observe the blue shift of 2D peak in three- to six-layer areas and the I_{2D}/I_G ratios are all higher than 2:1 as well.[34] The asymmetric 2D peaks in three- to six-layer areas could be split into two Lorenz peaks $2D_1$ and $2D_2$.[35] Due to the interlayer tunneling, the multilayers would open up new conducting channels for the charge carriers,[36,37] which may disturb the homogenous transport properties of the single-crystalline graphene. However, our measurements with varied geometry factors confirm the high homogeneity of transport properties of the graphene flake within measurement error.

To further investigate the effect of multi-layer graphene islands on transport property of graphene flake, local transport properties around these area are investigated, as shown in Fig. S6. Comparing with the graphene flake edge (Fig. S6(a)) which is far away from multi-layer graphene islands, the Dirac voltage is shifted to -20 V and the mobilities of both holes and electrons decrease by half, as shown in Fig. S6(b). In addition, according to pervious reports,[21,30] the graphene wrinkles would only influence the local resistivity. This suggests that graphene wrinkles and multi-layer islands act as localized carrier scatters. Since our measurements via van der Pauw geometry reveal the averaged properties of the macroscopic flake, its homogeneity may not be disturbed by these local factors. To fully understand the mechanisms behind this homogeneity, further investigations by scanning tunneling spectroscopy or scanning tunneling potentiometry are needed.[21]

4. Conclusions

In this study, we perform direct four-probe measurements on millimeter-sized single-crystalline graphene on SiO_2/Si substrate by a home-designed 4P-STM via van der Pauw geometry. The STM, optical, and Raman characterizations verify the continuity, high quality, and the monolayer nature of the graphene flake. The consistencies of conductivity and mobility between three setups confirm the high homogeneity of transport properties of the graphene flake. Our results also verify that the graphene wrinkles and small multilayered flakes do not disturb the homogenous transport properties of the total single-crystalline graphene flake. This non-invasive method may also be extended to analyzing the overall transport properties of other 2D materials.

Acknowledgment

The authors would like to thank Prof. Sokrates Pantelides for his valuable suggestion.

Appendix A. Supporting information

Supplementary material (STM imaging of graphene on Cu foil, optical and AFM imaging of graphene on SiO_2/Si substrate) is available.

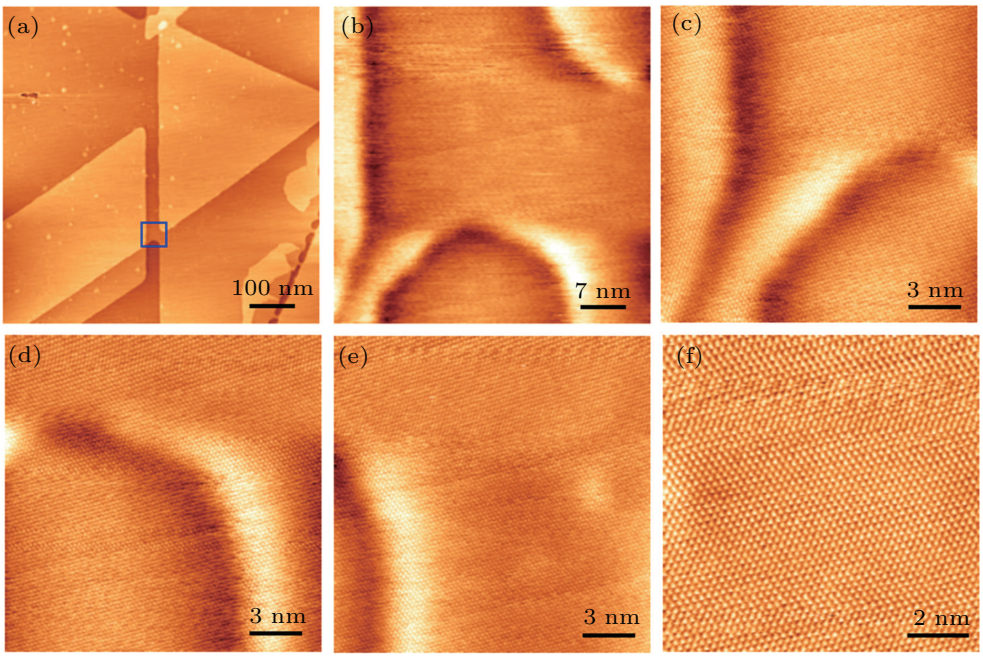


Fig. S1. (color online) STM characterization of graphene on Cu foil. (a): Large-area STM image on Cu foil. Parallelogram and triangular structures can be seen in this image. (b): Zoom-in STM image of the area indicated by a blue square in panel (a). (c)–(f): Atomically-resolved STM images within the region shown in panel (b). The triangular structures of graphene lattices are found to cover the fluctuant Cu surface continuously without any defect. These images verify the continuity and high quality of graphene grown on Cu foil. Scanning conditions: (a)–(f) $I_t = 369.4$ pA and $V_{sample} = 314.8$ mV.

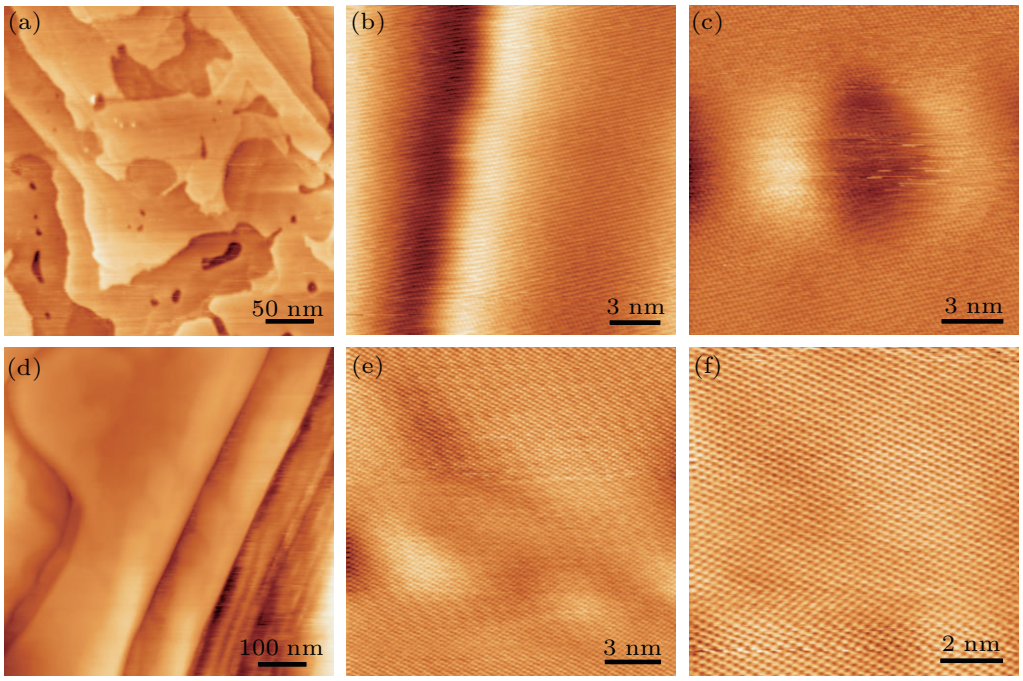


Fig. S2. (color online) STM characterizations of graphene on other structures in Cu foil. (a): STM topographic image of one typical structure on Cu foil. Irregular steps with complex shapes and small pits can be revealed in this image. (b): Atomic-scale STM image of graphene across a step in panel (a). (c): Atomic-scale STM image around a pit in panel (a). (d): Large-scale STM image of other structures on Cu foil. (e)–(f): Atomically-resolved STM images on the flat area in panel (d). Honeycomb structures can be clearly resolved in panel (f). The continuities of defect-free graphene lattices shown in panels (b), (c), (e), and (f) also verify the continuity and high quality of the sample. Scanning conditions: (a): $I_t = 300$ pA and $V_{sample} = 60$ mV. (b) and (c): $I_t = 520$ pA and $V_{sample} = 60$ mV. (d): $I_t = 358.6$ pA and $V_{sample} = 87.16$ mV. (e)–(f): $I_t = 823.9$ pA and $V_{sample} = 89.12$ mV.

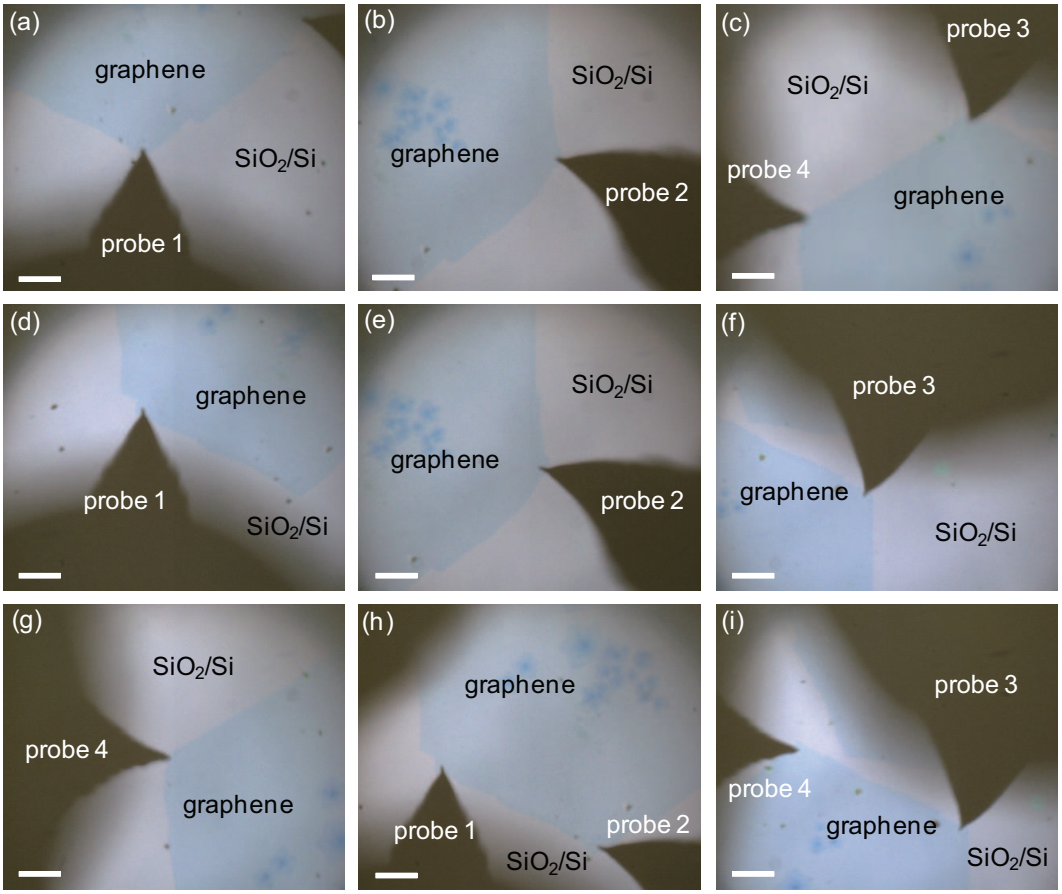


Fig. S3. (color online) Optical micrographs of probes during the four-probe measurements. (a)–(c): Optical micrographs showing the probes 1–4 contacting the graphene corners in setup-1. (d)–(g): Optical images of four probes during measurements in setup-2. (h) and (i): Optical images of four-probe measurements in setup-3. Chemical-etched gold probes are used in the measurements. Scale bar: 200 μm.

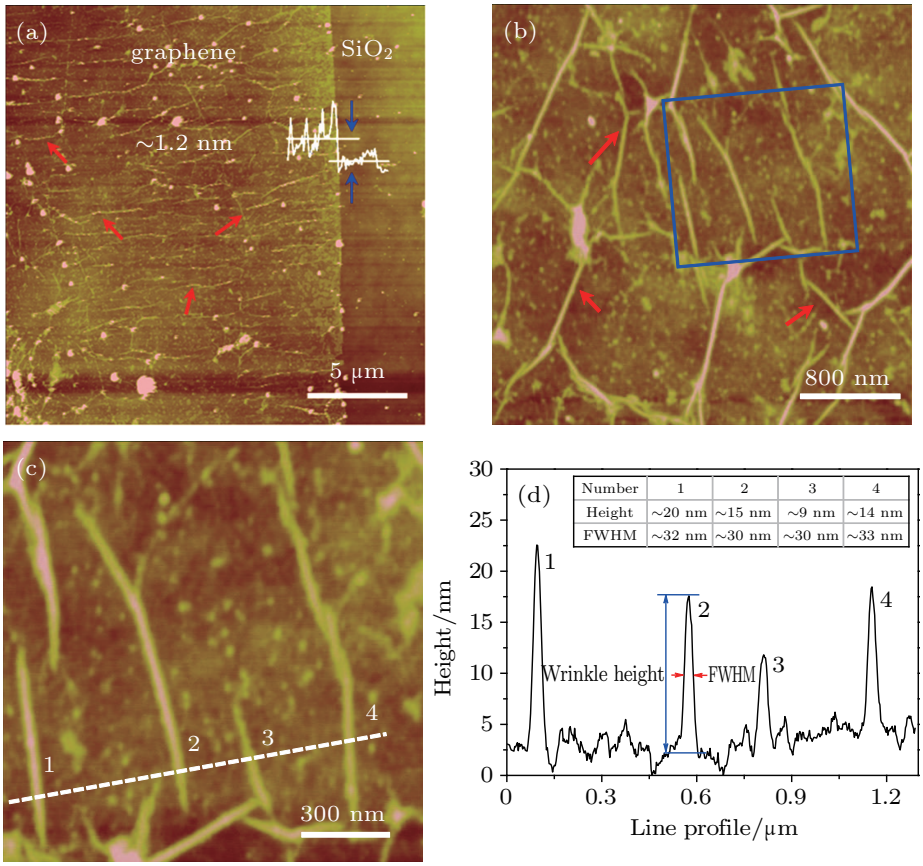


Fig. S4. (color online) AFM characterization of graphene on SiO_2/Si. (a): AFM height image of the graphene flake shown in Fig. 2. The graphene edge can be identified and the line profile reveals the thickness of this transferred graphene flake to be about 1.2 nm. Wrinkles indicated by red arrows can be found in this transferred graphene. (b): AFM image of the region near the center of the same graphene flake. (c): Magnified AFM image of the region indicated by a blue square in panel (b). (d): Line profile of the graphene wrinkles along the dash line shown in panel (c). The height and full width at half maximum (FWHM) of four wrinkles numbered in panel (c) are summarized in the inset table.

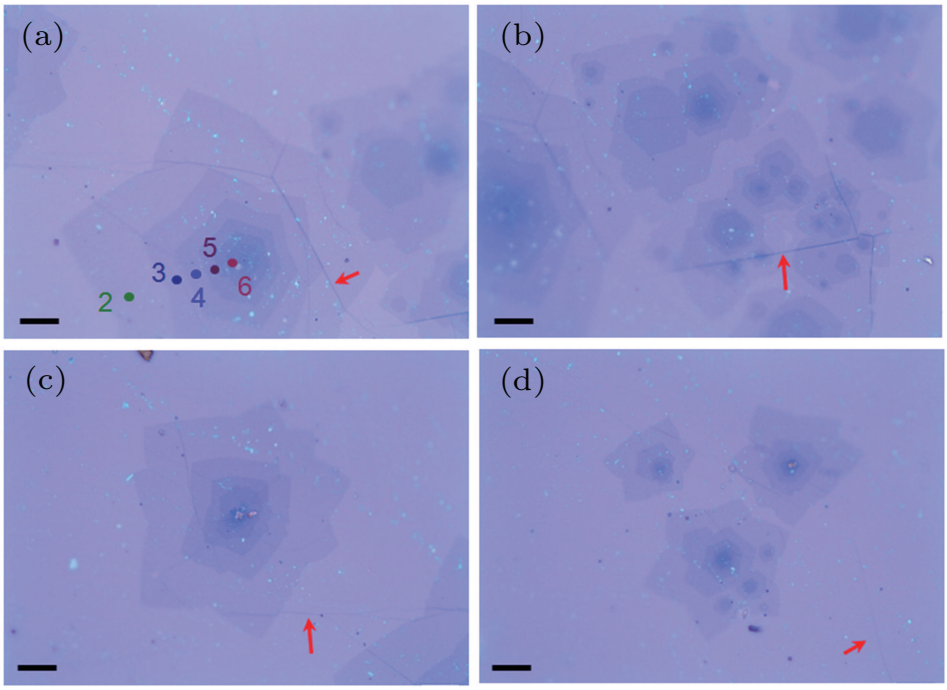


Fig. S5. (color online) Optical micrographs of small multi-layered graphene flakes. (a) and (b): Zoom-in optical micrographs showing the multilayers pointed by the left blue arrow in Fig. 2(a). The circles in panel (a) indicate the positions where the Raman spectra in Fig. 2(b) are collected. (c) and (d): Magnified optical images of graphene multilayers indicated by the middle and right blue arrow in Fig. 2(a), respectively. Graphene wrinkles indicated by red arrows can also be found in these optical images. Scale bar: 20 μm.

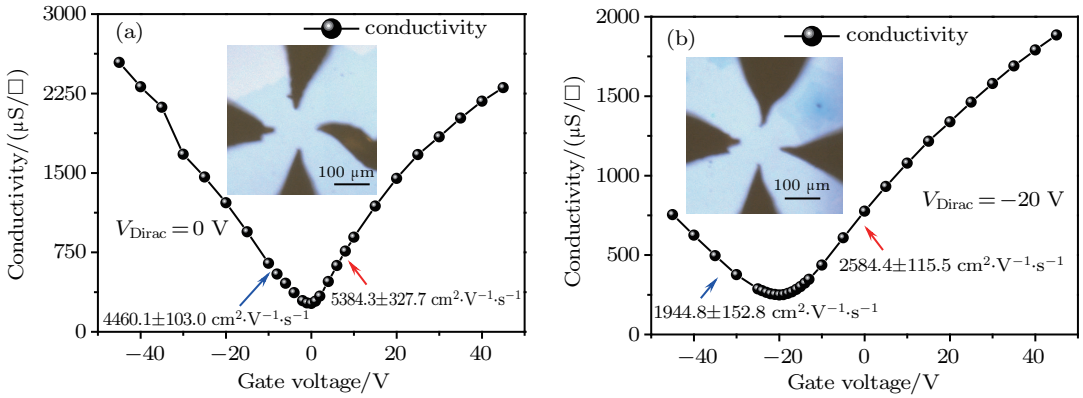


Fig. S6. (color online) Local transport properties of the millimeter-sized graphene flake. (a): Plot of conductivities versus gate voltage, measured near the edge of the graphene flake. The inset micrograph shows the positions of the four probes during measurements. The extracted hole and electron mobility are 4460.1±103.0 cm^2·V^{-1}·s^{-1} and 5384.3±327.7 cm^2·V^{-1}·s^{-1}, respectively. The Dirac voltage is at 0 V, indicating the high quality of single crystalline graphene flake. (b): Variation of conductivities with gate voltage, measured in the middle of the graphene flake near the multi-layer graphene islands. The inset show the micrograph during four-probe measurements. The extracted hole and electron mobility are 1944.8±152.8 cm^2·V^{-1}·s^{-1} and 2584.4±115.5 cm^2·V^{-1}·s^{-1}, respectively. The Dirac voltage is located at −20 V.

References

[1] Geim A K and Novoselov K S 2007 *Nat. Mater.* **6** 183
[2] Lee C, Wei X D, Kysar J W and Hone J 2008 *Science* **321** 385
[3] Novoselov K S, Geim A K, Morozov S V, Jiang D, Zhang Y, Dubonos S V, Grigorieva I V and Firsov A A 2004 *Science* **306** 666
[4] Bonaccorso F, Sun Z, Hasan T and Ferrari A C 2010 *Nat. Photon.* **4** 611
[5] Schwierz F 2010 *Nat. Nanotechnol.* **5** 487
[6] Yin Z Y, Zhu J X, He Q Y, Cao X H, Tan C L, Chen H Y, Yan Q Y and Zhang H 2014 *Adv. Energy Mater.* **4** 1300574
[7] Kim K S, Zhao Y, Jang H, Lee S Y, Kim J M, Kim K S, Ahn J H, Kim P, Choi J Y and Hong B H 2009 *Nature* **457** 706
[8] Guo W, Jing F, Xiao J, Zhou C, Lin Y W and Wang S 2016 *Adv. Mater.* **28** 3152
[9] Boyd D A, Lin W H, Hsu C C, Teague M L, Chen C C, Lo Y Y, Chan W Y, Su W B, Cheng T C, Chang C S, Wu C I and Yeh N C 2015 *Nat. Commun.* **6** 6620
[10] Mayorov A S, Gorbachev R V, Morozov S V, Britnell L, Jalil R, Ponomarenko L A, Blake P, Novoselov K S, Watanabe K, Taniguchi T and Geim A K 2011 *Nano Lett.* **11** 2396
[11] Du J, Li J Y, Kang N, Lin L, Peng H L, Liu Z F and Xu H Q 2016 *Nanotechnology* **27** 245204
[12] Miccoli I, Edler F, Pfnur H and Tegenkamp C 2015 *J. Phys.: Condens. Matter* **27** 223201
[13] Van der Pauw L J 1958 *Philips Technol. Rev.* **20** 220
[14] Van der Pauw L J 1958 *Philips Res. Rep.* **13** 1
[15] Dorgan V E, Bae M H and Pop E 2010 *Appl. Phys. Lett.* **97** 082112
[16] Lin X, He X B, Lu J L, Gao L, Huan Q, Shi D X and Gao H J 2005 *Chin. Phys.* **14** 1536
[17] Zou Q, Liu M, Wang G Q, Lu H L, Yang T Z, Guo H M, Ma C R, Xu X, Zhang M H, Jiang J C, Meletis E I, Lin Y, Gao H J and Chen C L 2014 *ACS Appl. Mater. Interfaces* **6** 6704
[18] Guo Q, Qin Z, Huang M, Mantsevich V N and Cao G 2016 *Chin. Phys. B* **25** 036801
[19] Nakayama T, Kubo O, Shingaya Y, Higuchi S, Hasegawa T, Jiang C S, Okuda T, Kuwahara Y, Takami K and Aono M 2012 *Adv. Mater.* **24** 1675
[20] Higuchi S, Kubo O, Kuramochi H, Aono M, Nakayama T 2011 *Nanotechnology* **22** 285205
[21] Clark K W, Zhang X G, Vlassiouk I V, He G W, Feenstra R M and Li A P 2013 *ACS Nano* **7** 7956
[22] Zhang Y F, Gao T, Gao Y B, Xie S B, Ji Q Q, Yan K, Peng H L and Liu Z F 2011 *ACS Nano* **5** 4014
[23] Blake P, Hill E W, Neto A H C, Novoselov K S, Jiang D, Yang R, Booth T J and Geim A K 2007 *Appl. Phys. Lett.* **91** 063124
[24] Ferrari A C, Meyer J C, Scardaci V, Casiraghi C, Lazzeri M, Mauri F, Piscanec S, Jiang D, Novoselov K S, Roth S and Geim A K 2006 *Phys. Rev. Lett.* **97** 187401
[25] Jiang Z, Zhang Y, Tan Y W, Stormer H L and Kim P 2007 *Solid State Commun.* **143** 14
[26] Pirkle A, Chan J, Venugopal A, Hinojos D, Magnuson C W, McDonnell S, Colombo L, Vogel E M, Ruoff R S and Wallace R M 2011 *Appl. Phys. Lett.* **99** 122108
[27] Tien D H, Park J Y, Kim K B, Lee N and Seo Y 2016 *Sci. Rep.* **6** 25050
[28] Choi M S, Lee S H and Yoo W J 2011 *J. Appl. Phys.* **110** 073305
[29] Li X L, Han W P, Wu J B, Qiao X F, Zhang J and Tan P H 2017 *Adv. Funct. Mater.*, January, 2017
[30] Vasic B, Zurutuza A and Gajic R 2016 *Carbon* **102** 304
[31] Zhu W J, Low T, Perebeinos V, Bol A A, Zhu Y, Yan H G, Tersoff J and Avouris P 2012 *Nano Lett.* **12** 3431
[32] Wu Q, Jung S J, Jang S K, Lee J, Jeon I, Suh H, Kim Y H, Lee Y H, Lee S and Song Y J 2015 *Nanoscale* **7** 10357
[33] Subhedar K M, Sharma I and Dhakate S R 2015 *Phys. Chem. Chem. Phys.* **17** 22304
[34] Karamat S, Sonuşen S, Dede M, Uysallı Y, Özgönül E and Oral A 2016 *J. Mater. Res.* **31** 46
[35] Zeng J, Liu J, Zhang S X, Zhai P F, Yao H J, Duan J L, Guo H, Hou M D and Sun Y M 2015 *Chin. Phys. B* **24** 086103
[36] Nagashio K, Nishimura T, Kita K and Toriumi A 2010 *Jpn. J. Appl. Phys.* **49** 051304
[37] Fang X Y, Yu X X, Zheng H M, Jin H B, Wang L and Cao M S 2015 *Phys. Lett. A* **379** 2245